Title

Theoretical investigation of ultrasound-modulated Cerenkov luminescence imaging for higher-resolution imaging in turbid media.

Journal

Optics Letters, 43(15)

ISSN

0146-9592

Authors

Klein, Justin S
Mitchell, Gregory S
Stephens, Douglas N
et al.

Publication Date

2018-08-01

DOI

10.1364/ol.43.003509

Peer reviewed

HHS Public Access

Author manuscript

Opt Lett. Author manuscript; available in PMC 2019 August 01.

Published in final edited form as:

Opt Lett. 2018 August 01; 43(15): 3509–3512.

Theoretical investigation of ultrasound-modulated Cerenkov luminescence imaging for higher resolution imaging in turbid media

Justin S. Klein[*], **Gregory S. Mitchell**, **Douglas N. Stephens**, and **Simon R. Cherry**

Department of Biomedical Engineering, University of California at Davis, One Shields Avenue, Davis, CA 95616, USA

Abstract

Cerenkov luminescence imaging (CLI) is an optical technique for imaging radiolabeled molecules *in vivo*. It has demonstrated utility in both the clinical and preclinical settings and can serve as a substitute for nuclear imaging instrumentation in some cases. However, optical scattering fundamentally limits the resolution and depth of imaging that can be achieved with this modality. In this manuscript, we report numerical results that support the potential for ultrasound-modulated Cerenkov luminescence imaging (USCLI), a new imaging modality that can mitigate optical scattering. The technique uses an acoustic Held to modulate the refractive index of the medium and thus the intensity of Cerenkov luminescence in a spatially precise manner. This mechanism of contrast has not been reported previously. For a physiologically compatible ultrasound peak pressure of 1 MPa, ~0.1% of the Cerenkov signal can be modulated. Furthermore, our simulations show that USCLI can overcome the scattering limit of resolution for CLI and provide higher resolution imaging. For an ^{18}F point source centered in a 1 cm^3 simulated tissue phantom with a scattering coefficient of μ_s ‘ = 10 cm^{-1}, <2 mm full width at half max (FWHM) lateral spatial resolution is possible, a resolution 3 times finer than the same phantom imaged with CLI.

Keywords

(110.0110) Imaging systems; (110.7170) Ultrasound; (060.3735) Imaging through turbid media

Cerenkov luminescence is optical radiation induced by fast charged decay particles emitted from a radioactive source [1] or produced during radiotherapy [2]. It has garnered growing interest owing to its lower cost, higher speed, and relative simplicity of instrumentation compared to traditional nuclear imaging methods such as PET or SPECT. However, like other *in vivo* optical imaging techniques, CLI is fundamentally limited in resolution and sensitivity by the optical properties of the tissue. These limitations will likely confine applications of CLI to the preclinical domain [1], to imaging radionuclides or radiation beams at shallow depths [3,4], or for radiotherapy beam profiling in transparent phantoms [5,6].

[*]Corresponding author: klein@ucdavis.edu.

In this Letter, we report a theoretical investigation of a new imaging technique, ultrasound-modulated Cerenkov luminescence imaging (USCLI), and present simulation results showing improved imaging resolution in turbid media. USCLI works by temporally modulating the generation of Cerenkov luminescence at a precise spatial location in the sample volume. The amplitude of the modulated signal is dependent on the flux of Cerenkov-producing charged particles in the interrogated volume and, consequently, concentration of a radionuclide or intensity of a traversing radiation beam. The modulated Cerenkov luminescence is detected with a non-imaging detector.

USCLI takes advantage of the refractive index- dependence of Cerenkov photon production and uses a focused acoustic wave that modulates the refractive index of a medium via the acousto-optic effect [7]. Modulating the refractive index, therefore, also modulates generation of the Cerenkov signal [1]. The key benefit of this method is that it shifts the dependence of spatial resolution from optical properties of the sample to the properties of the acoustic beam. Ultrasound focal volumes can be small and are unaffected by tissue optical properties. By scanning the focal volume of an ultrasound transducer over a sample containing a radiation source that produces Cerenkov luminescence, it is theoretically possible to determine the spatial location and relative intensity of the source, even in turbid media.

In a dark environment, an ultrasound transducer is rastered over the object of interest while a sensitive, non-imaging optical detector observes the object [Fig. 1]. Superposition of the ultrasound focal volume and radionuclide concentration determine the modulation of the optical signal, represented as a peak in the frequency domain of the detected signal, similar to [8]. The amplitude of the modulated frequency component is proportional to the concentration of radionuclide. Plotting each modulation amplitude (y axis) as a function of ultrasound position (x axis) creates a line profile of the radionuclide distribution. Three-dimensional images can be formed by combining multiple line scans.

Both analytical and Monte Carlo-based methods were used to numerically investigate USCLI. First-order feasibility was investigated by considering a simplified analytical model of a single, small, Cerenkov luminescence-generating volume [Fig. 2(a)] in order to understand the fundamental physics of contrast. For greater accuracy, a detailed Monte Carlo-based simulation was developed [Fig. 2(b)]. This simulation accounted for all relevant physics, including the geometry of ultrasound excitation and the propagation of electrons, positrons, and optical photons.

Analytical calculations considered a 250 **μ**m cube modulated by an overpressure [Fig. 2a)]. Cube dimensions were chosen to be smaller than the wavelength of a 1 MHz ultrasound transducer in tissue. Typical medical ultrasound frequencies range from ~1–20 MHz, corresponding to 1500–75 μm wavelength in tissue [9]. Cerenkov photons were generated from beta particles, defined to be either electrons or positrons, traversing the cube. The cube had the material properties of water (density = 1 g/mL) and refractive index of tissue (n=1.4). Equations from prior work [10,11] were used to compute the pressure-dependence of absorption coefficient (μ_a), scattering coefficient ($|\mu_s'$), and refractive index (n). Cerenkov photon yield was computed by numerically integrating $\frac{dN}{dx} \times \frac{dR}{dE'}$ the product of the Frank-

Tamm formula [1] and the derivative of an empirical fit to the range-energy relationship for beta particles [12]. This formulation accounts for the continuous loss of beta particle energy and the resulting instantaneously changing light yield. Beta particles and photons were assumed to ballistically traverse the full 250 μm side dimension of the cube [Fig 2a)]. To quantify the number of Cerenkov photons that could be "detected" from the cube, the generated photons were scaled by a term accounting for detection probability. Probability of being detected was computed using a modified Beer-Lambert formula and pressure-dependent μ_a, according to: $P_{detected} = e^{-\mu a x}$, where $x = 250$ μm.

Monte Carlo simulations were developed using GAMOS 5.0 [13] and the Tissue Optics plugin [14]. GAMOS is a framework which uses GEANT4 [15], a Monte Carlo software package that simulates the physics of nuclear decay, particle transport and optical photon transport. The simulation geometry [Fig. 2(b)] is a 1 cm^3 tissue phantom with a ^{18}F point source centered in the volume. ^{18}F is commonly used in nuclear medicine, and the energy spectrum of its decay beta particles is peaked at approximately the threshold for creation of Cerenkov radiation in water (suggesting that the isotope is a good candidate for observing effects of modulating the index of refraction and thus the threshold of the medium). The focal volume of an ultrasound transducer is simulated and stepped up to 5 mm, perpendicular to the acoustic axis, in 250 μm increments. The phantom consisted of 250 μm voxels with initial optical properties of: absorption coefficient $\mu_{a0} = 0.02$ cm^{-1}, reduced scattering coefficient μ_{s0} ' = 0 cm^{-1} or 10 cm^{-1}, and refractive index $n0$ =1.4. These were considered constant over the 400–800 nm wavelength range considered. A phantom with ultrasound- modulated optical properties was generated for one ultrasound cycle, with a sampling period of $\pi/10$ radians (equating to 20 time frames per cycle). Phantoms were generated by first computing ultrasound fields using FOCUS [16–18], a MATLAB-based software package for ultrasound field simulation (available at http://www.egr.msu.edu/~fultras-web/). Custom software written in MATLAB computed optical properties for each voxel based on equations from the literature [11] and the FOCUS- computed ultrasound pressure field. Computed fields corresponded to a 1 MHz, spherical, 7.7 mm focal depth, 19 mm diameter ultrasound transducer. A relatively high peak pressure of 10 MPa was used to reduce the number of particles simulated to a computationally manageable level. In a real experiment, this pressure would exhibit non-linear effects and likely cause cavitation. Results at this pressure can later be linearly scaled to lower levels. The ultrasound field had ~1.4 mm full width at half max (FWHM) average pressure amplitude beam diameter and a ~4.8 mm FWHM on-axis average pressure amplitude. For every combination of position and time point, 10^6 ^{18}F decays were simulated. All six outer surfaces of the phantom volume act as ideal detectors to score spatial coordinates, trajectory, wavelength, and a unique track number for Cerenkov photons. Data were used to generate Cerenkov luminescence images or summed to simulate the signal of a non-imaging detector. Cerenkov luminescence images were created by first repositioning incident photons to simulate an ideal lens then binning positions into 2D histograms with $(250\ \mu m)^2$ bins. The ideal lens was simulated by computing the photon's vector as follows: $\overrightarrow{V} = f \times \hat{d}$, where f is the 5 mm focal length of the simulated lens and $\hat{d}$ is the unit direction of the incident photon. Incident photon positions are offset by the photon's vector. A non-imaging detector was simulated by summing all counts in a given time bin. Time-resolved non-imaging count data were also processed with

a software heterodyne detector that outputted the amplitude and phase of the 1 MHz modulated optical signal.

Calculations of pressure-dependence of optical properties not shown) were in exact agreement with previous work [11]. Scattering and absorption coefficients are the most sensitive to pressure, and refractive index is the least. All optical properties increase linearly with pressure. Modulation of Cerenkov photon generation is most sensitive to overpressure for beta particles with lower energies that are close to the Cerenkov production threshold (~220 keV at n=1.4) [Fig. 3(a)]. Lower refractive index media are more sensitive to changes in pressure [Fig. 3(b)]. Fig. 3(c) demonstrates the pressure-dependence of photons escaping the volume and accounts for refractive index and absorption effects but not scattering. At low values of μ_{s0}' (<~35 cm^{-1}), increase in Cerenkov photon production is the dominant effect resulting in a positive fractional change in Cerenkov signal with increasing pressure. However, at higher absorption coefficients, with a relative loss in the detected signal, a negative fractional change in Cerenkov photons indicates that increase in absorption is the dominant effect of increased pressure.

Results were analyzed from two simulations (μ_{s0}'= 0 or 10 cm^{-1}) with tissue-like phantoms constructed from initial optical properties of μ_{a0} = 0.02 cm^{-1} and n_0 = 1.4. Spatially integrating the signal over one period of the ultrasound excitation for transducer positions 0 mm, 1 mm, and 2 mm [Fig. 4a)] demonstrates that ultrasound modulation of the Cerenkov signal is greatest when the ultrasound focal volume maximally overlaps with the ^{18}F source (0 mm, top left). Modulation decreases as the offset increases. No obvious modulation of the Cerenkov signal is present when the offset reaches 2 mm. Cerenkov luminescence images of the ^{18}F point source show that the μ_{s0}' = 10 cm^{-1} condition [Fig. 4(b), right] appears blurred relative to the μ_0' = 0 cm^{-1} condition [Fig. 4(b), left], due to optical scattering. Finally, [Fig. 4(c)] shows a comparison of point spread functions (PSFs) of conventional unmodulated CLI and modulated USCLI. For both conditions, USCLI produces narrower PSFs (~2 mm FWHM) compared to the unmodulated imaging case (6 mm FWHM) for this 5 mm deep point source. The narrower PSFs indicate higher spatial resolution.

We also consider if USCLI could be practically performed in a reasonable imaging timeframe. At a physiologically compatible US center frequency of 1 MHz and peak pressure of 1 MPa [9], ~0.1% of emitted Cerenkov photons are modulated (Fig. 4(c) linearly scaled to 1 MPa). This corresponds to a mechanical index of ~ 1, which is below the upper safety limit of 1.9 recommended for US imaging [9]. Contrast-to-noise ratio (CNR) is computed as follows [19]: $CNR = f\sqrt{C}$, where C are total counts observed and f is the fraction modulated.

For a small animal imaging case, if we assume a 3.7 MBq injected dose (I.D.) and activity concentration of 10% I.D./g, a 179 mm^3 tumor (7 mm diameter sphere) would weigh 179 mg and contain 66 kBq of ^{18}F. Each decay would generate ~2 optical photons [20], corresponding to a Cerenkov flux of ~132,000 photons/second. To reach a CNR > 2, 4 M counts would need to be observed. Assuming a perfect, shot noise limited imaging system, 30 seconds of acquisition time would be required. Thus, to form a three dimensional image of even a mouse-sized object by rastering a small focal volume would require a large amount

of time with the proposed scheme. For practical use, methods to decrease acquisition times likely would need to be developed.

In summary, analytical calculations performed on a simplified model and detailed Monte Carlo simulation support the possibility of USCLI. The data suggest that USCLI achieves higher spatial resolution imaging compared to conventional CLI in the presence of optical scattering. USCLI relies on a new and unreported mechanism of imaging contrast: acoustic pressure spatial-temporally modulating the refractive index of a medium, leading to a modulation of Cerenkov photon generation. This signal is localized to the focal volume of the ultrasound transducer, which can be <1 |μL in volume. Our simulations demonstrate that the modulated signal depends on μ_{a0}, μ_{s0}, n_0, and beta particle energy. Larger changes in the Cerenkov signal are observed for lower refractive indices and kinetic energies closer to the threshold. For a reasonable range of tissue absorption coefficients (μ_{a0} = 0.1 to ~35 cm^{-1}) [21], acoustic overpressure produces a positive fractional change in the Cerenkov signal. For a physiologically compatible acoustic overpressure of 1 MPa, 0.1% of the generated Cerenkov signal is modulated a smaller fraction of this is detectable, depending on optical properties and source depth).

It will be challenging to apply USCLI to *in vivo* imaging. The Cerenkov signal is weak, already requiring sensitive cameras and modest integration times to obtain images with reasonable CNR. The disadvantage of our method, as currently proposed, is the need to raster the ultrasound beam point-by-point over the sample in order to form an image. This theoretical investigation has provided quantitative insight into the physics of its mechanism of contrast. Work is already underway to experimentally demonstrate this imaging approach. In principle, it should be possible to probe multiple volumes of interest simultaneously using a range of ultrasound excitation frequencies. This could dramatically increase the speed of this technique, moving toward the realm of biologically practical imaging times.

Acknowledgment.

Justin Klein was supported by a fellowship from the Society of Nuclear Medicine and Molecular Imaging and Education Research Foundation. We acknowledge Pedro Arce and Adam Glaser for GAMOS and Tissue Optics plugin support. Laboratory mouse vector graphic used in Figure 1 is from Wikimedia Commons user Gwilz, licensed under CC-BY-SA-4.0.

Funding. National Institutes of Health (NIH) grant R35 CA197608.

References

1. Mitchell GS, Gill RK, Boucher DL, Li C, and Cherry SR, Philos. Transact. A Math. Phys. Eng. Sci 369, 4605–4619 (2011).
2. Axelsson J, Davis SC, Gladstone DJ, and Pogue BW, Med. Phys 38, 4127–4132 (2011). [PubMed: 21859013]
3. Holland JP, Normand G, Ruggiero A, Lewis JS, and Grimm J, Mol. Imaging 10, 177–186 (2011). [PubMed: 21496448]
4. Liu H, Carpenter CM, Jiang H, Pratx G, Sun C, Buchin MP, Gambhir SS, Xing L, and Cheng Z, J. Nucl. Med 53, 1579–1584 (2012). [PubMed: 22904353]
5. Glaser AK, Davis SC, McClatchy DM, Zhang R, Pogue BW, and Gladstone DJ, Med. Phys 40, 012101 (2013). [PubMed: 23298103]

6. Glaser AK, Davis SC, Voigt WHA, Zhang R, Pogue BW, and Gladstone DJ, Phys. Med. Biol 58, 601 (2013). [PubMed: 23318469]
7. Kao K-C, Dielectric Phenomena in Solids: With Emphasis on Physical Concepts of Electronic Processes (Academic Press, 2004).
8. Jarrett CW, Caskey CF, and Gore JC, PLoS ONE 9, e104268 (2014). [PubMed: 25105880]
9. ter Haar Gail, The Safe Use of Ultrasound in Medical Diagnosis, 3rd ed (The British Institute of Radiology, 2012).
10. Wang LV, Phys. Rev. Lett 87, 043903 (2001). [PubMed: 11461618]
11. Zhang Q, Mather ML, and Morgan SP, IEEE Trans. Biomed. Eng 62, 2135–2143 (2015). [PubMed: 25706504]
12. Ross HH, Anal. Chem 41, 1260–1265 (1969).
13. Arce P, Rato P, Canadas M, and Lagares JI, in IEEE Nuclear Science Symposium Conference Record, 2008. NSS '08 (2008), pp. 3162–3168.
14. Glaser AK, Kanick SC, Zhang R, Arce P, and Pogue BW, Biomed. Opt. Express 4, 741–759 (2013). [PubMed: 23667790]
15. Agostinelli S, Allison J, Amako K, Apostolakis J, Araujo H, Arce P, Asai M et al., Nucl. Instrum. Methods Phys. Res. Sect. Accel. Spectrometers Detect. Assoc. Equip 506, 250–303 (2003).
16. Kelly JF and McGough RJ in AIP Conference Proceedings (AIP Publishing, 2009), Vol. 1113, pp. 210–214.
17. Kelly JF and McGough RJ, IEEE Trans. Ultrason. Ferroelectr. Freq. Control 53, 1150–1159 (2006). [PubMed: 16846147]
18. Chen D and McGough RJ, J. Acoust. Soc. Am 124, 1526–1537 (2008). [PubMed: 19045644]
19. Cherry SR, Sorenson JA, and Phelps ME, Physics in Nuclear Medicine (Elsevier Health Sciences, 2012).
20. Gill RK, Mitchell GS, and Cherry SR, Phys. Med. Biol 60, 4263–4280 (2015). [PubMed: 25973972]
21. Jacques SL, Phys. Med. Biol 58, R37–R61 (2013). [PubMed: 23666068]

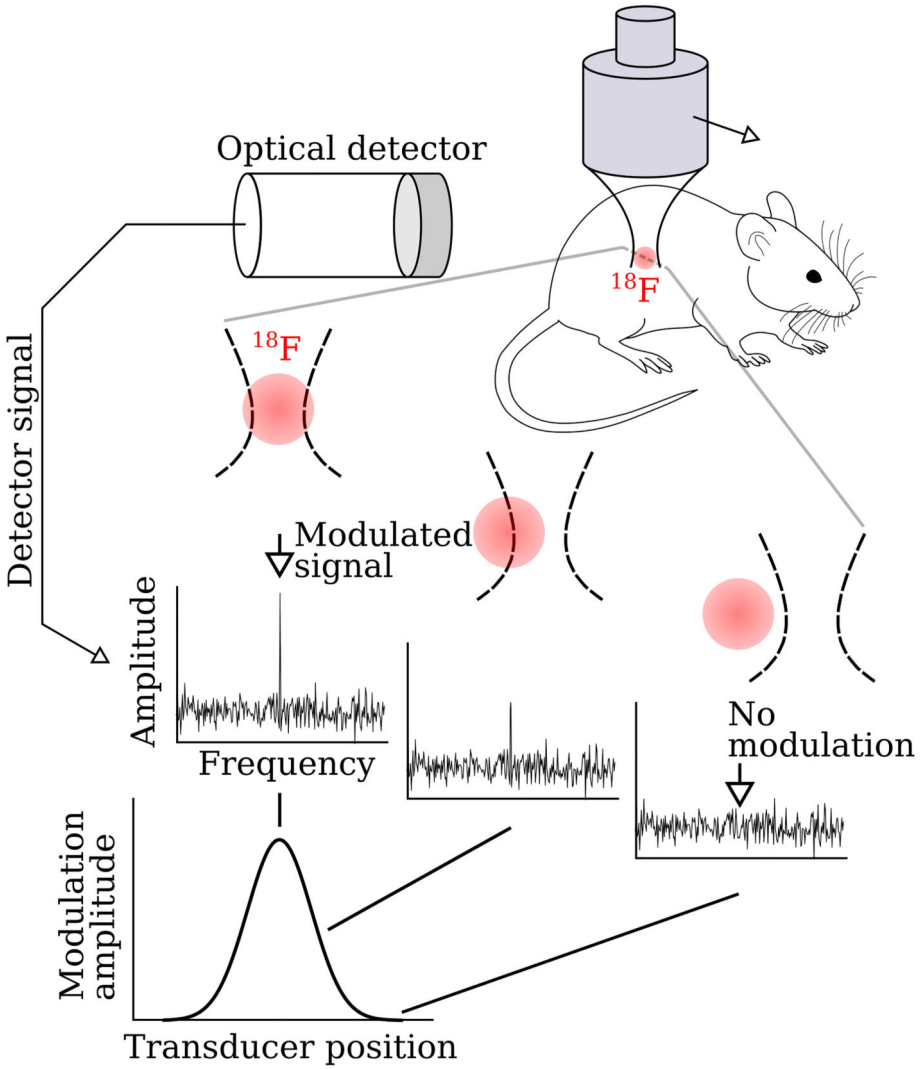

Fig. 1.

Concept for ultrasound modulated Cerenkov luminescence imaging. An object is scanned with a US field, which modulates the refractive index in the focal volume. Superposition of the ultrasound field and radionuclide (decreasing left to right in diagram), determines the strength of the modulated Cerenkov signal. The optical detector, observing the entire object, detects a signal at the frequency of the ultrasound transducer, with a magnitude proportional to the modulated optical signal (appearing as a peak in the frequency domain signal of the detector). Plotting the magnitude of the modulated signal as a function of the position of the ultrasound transducer will produce a profile of the radionuclide distribution. Many profiles are acquired to produce an image.

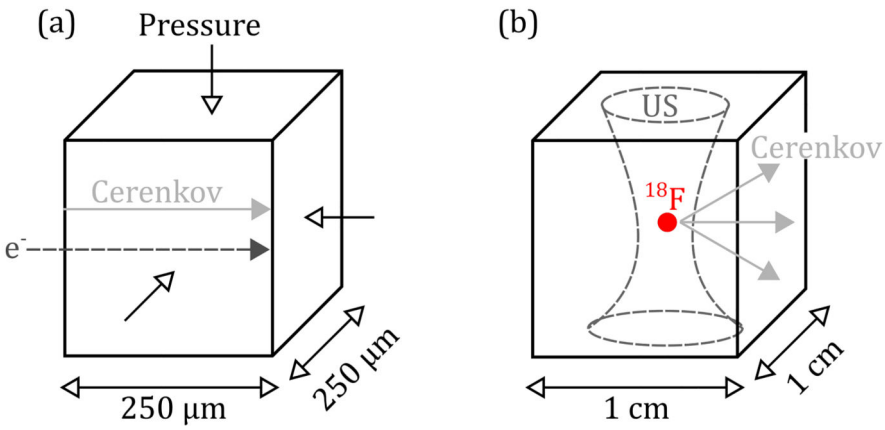

Fig. 2.

Geometries used for analytical calculations and Monte Carlosimulations. (a) Cerenkov emission in single pressure-modulated cube. A uniform overpressure (pressure above atmospheric) is applied to all faces of a 250 µm cube while monoenergetic beta particles traverse the cube perpendicular to a face and produce Cerenkov photons. (b) Monte Carlo simulation of ultrasound-modulated Cerenkov luminescence imaging. Optical properties in a 1 cm^3 phantom with 250 µm voxels are modulated by an ultrasound transducer pressure field (US). An ^{18}F point source is centered in the volume. Cerenkov photons propagate through the voxelized media and are scored if they reach surfaces of the phantom.

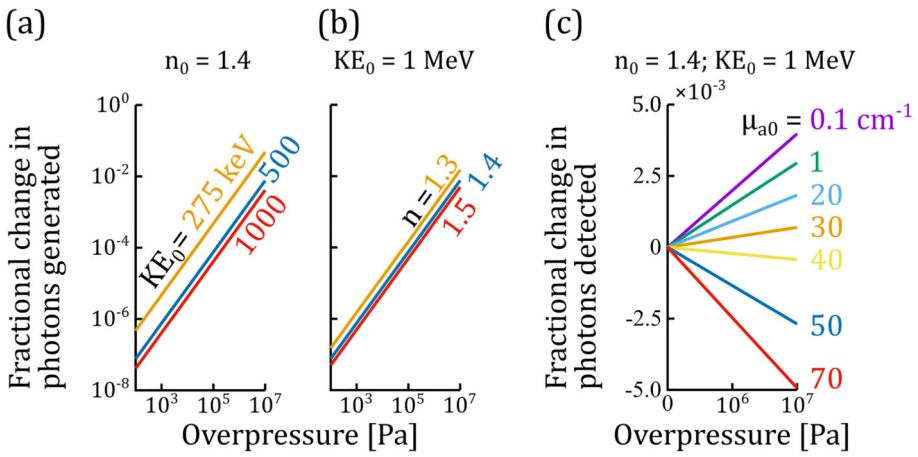

Fig. 3.

Pressure dependence of optical properties, generated Cerenkov photons, and detected Cerenkov photons. (a) Cerenkov photons produced from lower energy electrons are most sensitive changes in pressure. (b) Lower refractive index media produce larger changes in generated Cerenkov photons. Number of generated Cerenkov photons increases with pressure. (c) Number of detected Cerenkov photons increases with pressure when initial absorption coefficient of the tissue is <~35 cm^{-1}. In tissues with higher absorption coefficients, the change in detected Cerenkov photons is dominated by increased absorption.

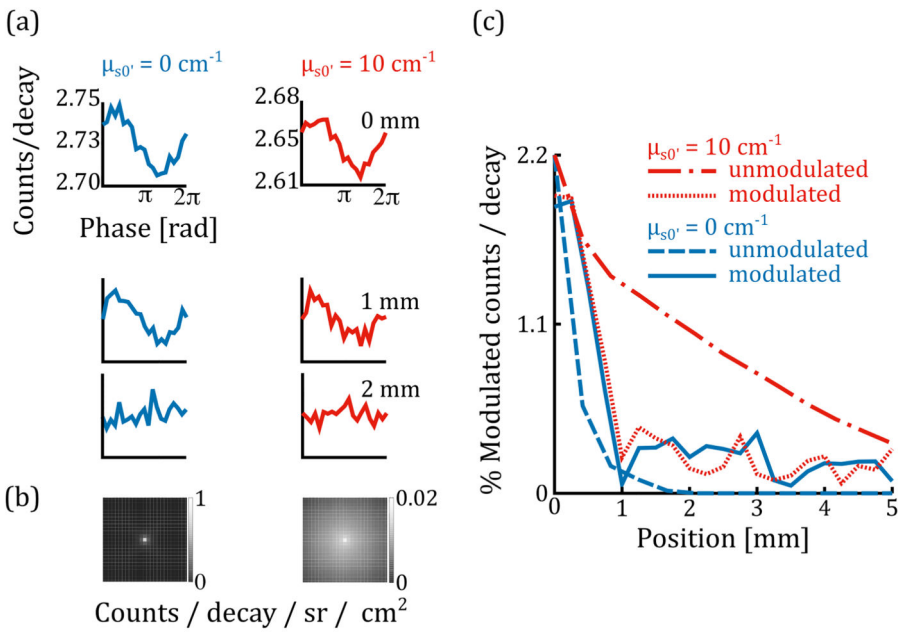

Fig. 4.

Ultrasound temporally modulates the Cerenkov signal, allowing higher resolution imaging in the presence of scattering (10 MPa, unsealed data). (a) spatially-integrated signal for 0 mm, 1 mm, and 2 mm ultrasound transducer positions. When the ultrasound focus is centered over the point source 0 mm offset), greatest temporal modulation of Cerenkov photons reaching the detector is observed; none is apparent when the US transducer is offset by 2 mm. (b) Cerenkov luminescence images of the point source demonstrated blurring due to range of the beta particle and due to scattering of Cerenkov photons in the case where the medium has a non-zero scattering coefficient (μ_{s0} = 10 cm-^{1}, right). (c) Comparison of normalized line profiles from Cerenkov luminescence images b) with magnitude of ultrasound-modulated Cerenkov luminescence signal. The width of the line profile, a measure of the point-spread function (PSF), increases in the presence of scattering for CLI, but not for USCLI.